Structural and magnetic characterization of the lithiated iron oxide $Li_xFe_3O_4$

J. Fontcuberta and J. Rodríguez
Facultat Fisica, Universitat Barcelona, Diagonal 645, Barcelona 08028, Spain and Escola Tecnica Superior d'Enginyers de Telecomunicacions, Universitat Politècnica de Catalunya, J. Girona s/n, Barcelona 08034, Spain

M. Pernet
Laboratoire Cristallographie, Centre National de la Recherche Scientifique, B.P. 166, Grenoble, France

G. Longworth and J. B. Goodenough
Nuclear Physics Division, Atomic Energy and Research Establishment, Harwell, Oxfordshire OX11 ORA, United Kingdom and Inorganic Chemistry Laboratory, South Parks Road, Oxford OX1 3QR, United Kingdom

(Received 24 June 1985; accepted for publication 24 October 1985)

The Rietveld profile-analysis method is used to investigate the x-ray diffraction pattern of lithiated Fe_3O_4. It is shown that, after exposure to air, pure magnetite coexists with a lithium-inserted $Li_xFe_3O_4$ phase. The Mössbauer spectra at 300 and 4.2 K have been used to estimate the lithium content of the sample, the pure magnetite concentration, and the iron distribution over the available 16*c* and 16*d* sites of the spinel structure. Magnetization measurements from 4.2 to 120 K with an external magnetic field up to 150 kOe have been used to obtain the saturation magnetic moment, the magnetic anisotropy constants, and the susceptibility. It is concluded that a noncollinear spin structure should be present in $Li_{0.5}Fe_3O_4$. These results indicate that there is no room-temperature extrusion of iron even for $x \to 2.0$, but that on exposure to air $Li_xFe_3O_4$ samples with $x > 0.5$ are oxidized at room temperature by delithiation.

INTRODUCTION

Room-temperature Li^+-ion mobility in a close-packed array of oxide ions is now well established. In the layered compounds $Li_{1-x}MO_2$ (M = V, Cr, Co, or Ni), there is a degree of freedom along the trigonal axis perpendicular to the layers, and a room-temperature chemical-diffusion coefficient $D = 5.0 \times 10^{-12}$ m^2/s for Li^+-ion motion in $Li_{1-x}CoO_2$ has been measured by pulse techniques[1] and by three independent methods with complex-impedance analysis.[2]

Lower, but nevertheless significant, three-dimensional Li^+-ion motion has been established in compounds with the $[B_2]O_4$ framework of an $A[B_2]O_4$ spinel.[3,4] The observation[5,6] of the room-temperature instability to oxidation in the spinel system $Li[Li_xTi_{2-x}]O_4$ first signaled that Li^+ ions are mobile at low temperatures in oxospinels, and independent electrochemical lithiation of Fe_3O_4 (Ref. 7) and $Li[Ti_2]O_4$ (Ref. 8) as well as chemical delithiation of $Li[Mn_2]O_4$ (Ref. 9) established that this is indeed the case.

Investigation of the process of lithiation in $Li_xFe_3O_4$ (Refs. 10 and 11), $Li_xMn_3O_4$, and $Li_{1+x}[Mn_2]O_4$ (Ref. 12) has led to the conclusion that the guest Li atoms enter the empty octahedral sites of the $A[B_2]O_4$ spinel structure, the sites 16*c* of space group $Fd3m$ (see Fig. 1), as Li^+ ions; their charge-compensating electrons reduce the host, but the $[B_2]O_4$ subarray is otherwise unperturbed. However, a strong electrostatic repulsion between an interstitial Li^+ ion on a site 16*c* and its two neighboring tetrahedral-site A cations on sites 8*a*, which share common faces with sites 16*c*, induces a displacement of the A cations from the 8*a* sites. Beyond a critical concentration x_c of interstitial Li, the cubic-close-packed oxide-ion array contains, in most cases, only octahedral-site cations. The atomic configuration is then $(Li_xA\square_{1-x})[B_2]O_4$, $x_c < x < 1$, where the parentheses enclose cations and vacancies $\square$ randomly distributed on sites 16*c* and the square brackets host B cations on 16*d* sites of the space group $Fd3m$. Thus room-temperature lithiation of an $A[B_2]O_4$ spinel to $(LiA)[B_2]O_4$ produces a rocksalt structure having a peculiar cation ordering.

In the case of $Li_xFe_3O_4$, room-temperature lithiation in excess of $x = 1$ was observed, and it was concluded[10] that in the compositional range $x > 1$ the $x - 1$ excess Li^+ ions oc-

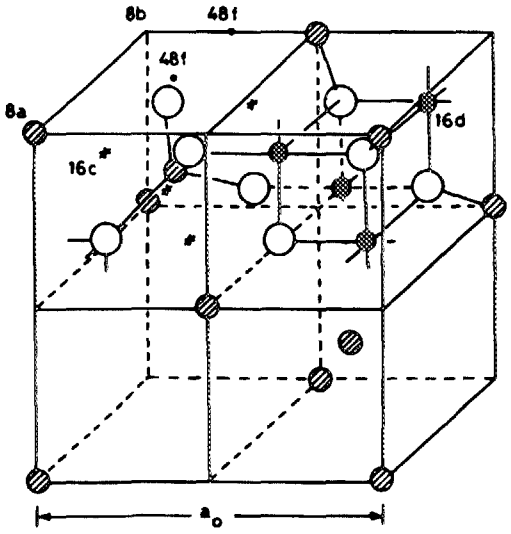

FIG. 1. Spinel unit cell. Only one-half is shown with respect to the 8*a* and 8*b* sites, and one-quarter with respect to the other sites.

 0021-8979/86/061918-09$02.40

cupy tetrahedral sites 8*a* and/or 48*f*. However, at higher temperatures (400 °C) extrusion of elemental iron made the lithiation process more complex;[11] this observation raises the possibility that iron extrusion also occurs at room temperature.

The initial room-temperature investigation[10] of lithiated magnetite $Li_xFe_3O_4$ did not permit an adequate determination of the crystallographic reliability factor or any other quality-of-fit parameter. In this paper we present data obtained from a quantitative fit of the complete x-ray-diffraction profile based on the Rietveld method.

This paper also reports for the first time preliminary Mössbauer and magnetization investigations of the magnetic properties of lithiated magnetite. From the spin-wave spectrum of ferrimagnetic Fe_3O_4, Torrie[13] has shown that the Fe_B-Fe_B interactions are weakly ferromagnetic; a high Curie temperature [$T_C = 850$ K (Ref. 14)] is due to the strong, antiferromagnetic Fe_A-O-Fe_B interactions. Displacement of the tetrahedral-site Fe_A iron to octahedral sites in lithiated $Li_xFe_3O_4$ would introduce a different magnetic order with the possibility of a different ferrimagnetism due to the unusual cation ordering present. Mössbauer data[15,16] have established the existence of fast electron transfer ($\tau < 10^{-8}$ s) between Fe_B ions at room temperature in $Fe_A^{3+}[Fe_B^{3+}Fe_B^{2+}]O_4$, but below the Verwey transition at $T_V = 120$ K discrete Fe_B^{3+} and Fe_B^{2+} species can be detected. The Mössbauer data provide an independent measure of the mean valence state, in the case of fast electron transfer, or the relative valence-state populations in the case of slow (relative to 10^{-7} s) electron transfer. They should also give independent evidence of any extruded metallic iron, which would generally be undetected by x-ray diffraction.

EXPERIMENTAL PROCEDURE

Lithiation of Fe_3O_4 (Cerac Inc., purity >99.5%, −325 mesh) was carried out chemically using *n*-butyl-lithium under a nitrogen atmosphere. Further details on the synthesis procedure can be found elsewhere.[10]

Chemical analysis of the $Li_xFe_3O_4$ sample was carried out by atomic-absorption spectroscopy. If it is assumed that the final compound is a single phase with a homogeneous Li distribution, an $x = 1.7$ value is obtained, corresponding to a compositional formula $Li_{1.7}Fe_3O_4$.

The x-ray-diffraction pattern was obtained on a Siemens D500 diffractometer with Cu$K\alpha$ radiation (1.5405 and 1.5443 Å) and a graphite analyzing monochromator. The data were collected with the usual step-scanning procedure ($\Delta\theta$ step = 0.04° time per step of 10 s) from 16° to 100° (2θ).

The Mössbauer spectra were taken at 300 and 4.2 K with ^{57}CoRh and ^{57}CoPd sources, 512 and 1024 channels respectively, and a constant acceleration drive system. Calibration was done with respect to α-Fe at room temperature. Thermomagnetic measurements were carried out in an extraction magnetometer (Service National Champs Intenses, Grenoble) in a temperature range from 4.2 to 120 K with an applied magnetic field up to 15 T.

X-RAY DIFFRACTION RESULTS

The data were analyzed with the DBW 3.2 version of the Wiles and Young program.[17] The quality-of-fit R factors used are defined in the usual way by

$$R_{wp} = 100\left(\sum_i w_i [Y_i(o) - Y_i(c)]^2 \Big/ \sum_i w_i [Y_i^2(o)]\right)^{1/2},$$

$$R_E = 100\left((N - P + C) \Big/ \sum_i w_i Y_i^2(o)\right)^{1/2},$$

$$R_B = 100 \sum_i |I_o - I_c| \Big/ \sum I_o,$$

where $Y_i(o)$ and $Y_i(c)$ are observed and calculated profile intensities, respectively, including background contributions; w_i is the weighting factor, which takes into account the counting statistics. N, P, and C are the number of scanning points, fitting parameters, and constraints, respectively. I_o and I_c are the observed and calculated integrated intensities of each Bragg reflection, respectively. The summation is over all the points in the scan for R_{wp} and R_E and over all the Bragg reflections for R_B, where R_{wp}, R_E, and R_B stand for the weighted pattern, expected, and Bragg quality-of-fit factors.

In the fitting procedure, asymmetry at lower angles and monochromator corrections were included. The background has been fitted with a polynomial function. The zero-point correction has also been included. In all refinements, only an overall isotropic temperature factor was used because the quality of the data was insufficient to justify the refinement of individual isotropic temperature factors.

The pseudo-Voigt profile function has been used, following Young and Wiles.[18] The fit has led to a pseudo-Voigt *n* factor very close to 1.00, which shows that equally good fits would be obtained with a Lorentzian profile.

Analysis of the data has carried out on the basis of the proposed room-temperature lithiation process[10] for the lithium incorporation. It can be summarized as follows:

$$(Fe^{3+})_{8a}[Fe_2^{3+/2+}]_{16d}O_4 \xrightarrow[x_c\ \mathrm{Li}]{} (Li_{x_c}^{+}Fe^{3+/2+})_{16c}[Fe_2^{3+/2+}]_{16d}O_4$$

$$\xrightarrow[1-x_c\ \mathrm{Li}]{\mathrm{I}} (Li^{+}Fe^{3+/2+})_{16c}[Fe_2^{3+/2+}]_{16d}O_4$$

$$\xrightarrow[1.0\ \mathrm{Li}]{\mathrm{II}} (Li^{+})_{8a,48f}(Li^{+}Fe^{2+})_{16c}[Fe_2^{2+}]_{16d}O_4$$

$$\xrightarrow[6.0\ \mathrm{Li}]{\mathrm{III}} 4\,Li_2O + 3\,Fe,$$

where x_c indicates a critical concentration ($x_c < 0.1$) above which a cooperative displacement of the 8*a* Fe^{3+} ions into the empty 16*c* positions takes place.

Our procedure was to investigate the profile-refinement data for the following structural models:

(i) $(Li_{x-1}Fe_y)_{8a}(LiFe_{1-y})_{16c}[Fe_2]_{16d}O_4$, $y < 2-x$, $x > 1$,

(ii) $(Li_{x-1-y}Fe_y)_{8a}(Li_{1+y}Fe_{1-y})_{16c}[Fe_2]_{16d}O_4$,

(iii) $(Li_{x-1-y})_{8a}\{Li_y\}_{48f}(LiFe)_{16c}[Fe_2]_{16d}O_4$,

(iv) α-$(Li_{x-1-y}Fe_y)_{8a}(Li_{1+y}Fe_{1-y})_{16c}[Fe_2]_{16d}O_4 + \beta$-$Fe_3O_4$.

In all four cases, the lithium concentration x is taken to be the value obtained from the chemical analysis. These four models support different physical situations that should be made clear. Model (i) allows an incomplete occupancy of the octahedral 16*c* positions and the coexistence of Fe in 8*a* and 16*c* positions. In model (ii) the cationic distribution is constrained to give complete occupancy of the 16*c* sites. Model (iii) allows the presence of Li in the empty tetrahedral 48*f* positions and constrains the Fe ions into octahedral positions, which are fully occupied. Finally, with model (iv) we investigate the presence of a pure magnetite phase together with the lithiated phase. In that case the actual value of x in the lithiated phase is dependent on β; in principle, it should be possible to estimate $\beta = 1 - \alpha$ by an iterative process. The reasons for considering this model are given below.

In Table I we summarize the values obtained for y, a, u, B, R_{wp}, and R_{expt} for all the models.

In Fig. 2 we show the fitted x-ray diffraction pattern for model (i) together with the pattern difference between the observed and calculated data. Inspection of the pattern difference clearly reveals that the calculated pattern is systematically displaced toward lower angles with respect to the experimental pattern. In addition, the computed intensities of the (111) and (220) lines are higher and lower, respectively, than the observed lines, suggesting that the occupation fraction of the Fe ions in the tetrahedral positions should be higher than the value obtained from the fitting.

The fits for models (ii) and (iii) reveal the same features; in addition, model (iii) leads to an unacceptable value of the lithium content (3.277 ions/formula unit) in the tetrahedral 8*a* positions and consequently a negative occupation of the 48*f* sites in order to preserve the total Li concentration in the sample. In this case, the x coordinate of the 48*f* position was kept fixed to its deal 3/8 value because it was impossible to reach a convergent fit when allowing free variations of this coordinate and because the R factors and the occupation fraction were insensitive to the x-coordinate value.

All these results show that, in a single-phase model, the 8*a* sites should be occupied by strong-scatterer ions (Fe^{m+}) or, alternatively, a second phase with occupied 8*a* positions should be present in the sample. It follows that another phase, presumably pure magnetite, can be present in our sample, which justifies the proposed model (iv). Moreover, in this type of experiment it has been commonly observed that some particles are not lithiated, especially if the particles are exposed to air.

In order to use model (iv), we started with the assumption that no Fe ions are in the 8*a* sites and that the octahedral 16*c* positions are full. The remaining lithium (0.7 per molecule) are incorporated into the tetrahedral 8*a* positions.

The fitting procedure for two phases has been carried out with the following fixed parameters: the lattice constant ($a = 8.396$ Å) and the oxygen parameter ($u = 0.254$) of pure magnetite.[19] In addition, in a first step we have assumed that the overall isotropic temperature factors for both phases are the same, and we have permitted independent variations of the half-width parameters.

The purpose of this fitting was to get the relative concentration of Fe_3O_4 in the sample from the overall scale factors obtained for each phase. With this model, the R_{wp} factor drops to 15.28; see Table I. The remarkably lower value obtained for R_{wp} confirms the presence of "unreacted" Fe_3O_4 in the sample. The concentration of magnetite obtained from the scale factors is about 15(2)%. Therefore, it follows that the Li concentration in the lithiated phase should be corrected to a new value $x = 2.0$ if all the Li is inserted into the lithiated particles.

Accordingly, the fitting process has been repeated with $x = 2$ and with the same restrictions and constraints in the adjustable set of parameters. As one could expect, due to the low scattering factor of the lithium, no significant difference in the R_{wp} factor (15.10) and in the Fe_3O_4 concentration [14.7(2.0)%] was found. In Fig. 3 we show the fitted pattern. Comparison with Fig. 2 clearly shows the improved quality of the fit.

In order to check the influence of the constraints on the

TABLE I. Parameters obtained from the fitting of the profile of the x-ray-diffraction pattern. y gives the cationic distribution. a(Å) and u are lattice and oxygen parameters, respectively. B(Å^2) is the temperature factor. R_{wp}, R_E, and R_B are quality-of-fit parameters as defined in the text.

Model	y	a (Å)	u	B (Å^2)	R_{wp}	R_E	R_B
(i)	0.175(6)	8.461(1)	0.2510(7)	0.7(1)	18.28	7.73	4.83
(ii)	0.192(6)	8.461(1)	0.2510(7)	0.7(1)	18.28	7.73	4.82
(iii)	−2.577(1)	8.460(1)	0.254 (1)	0.9(2)	18.75	7.73	5.01
(iv)	0.000	8.465(1)	0.2508(7)	0.5(1)	15.28	7.72	4.10

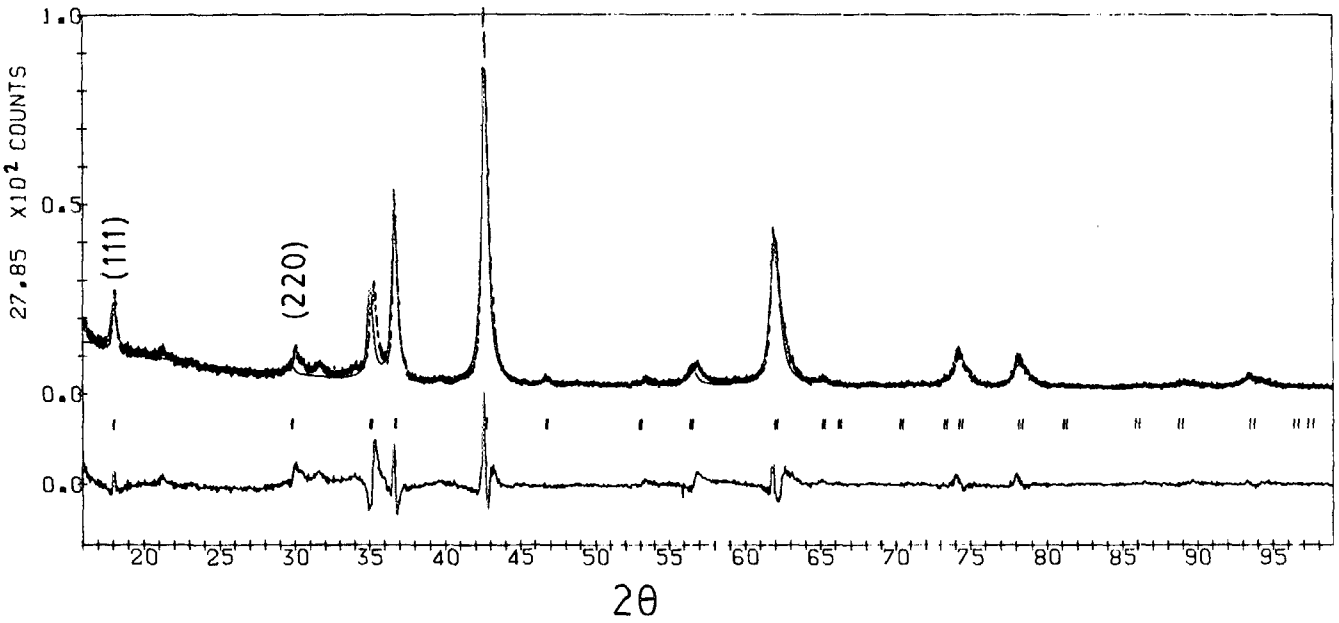

FIG. 2. X-ray diffraction pattern for $Li_xFe_3O_4$, fitted with model (i).

fit, we have run a new set of refinements that allow for free variations of the overall temperature factors, but keep equal the variations and values of the half-width parameters. This procedure gives $R_{wp} = 15.28$ and 17(2)% of magnetite.

In summary we can conclude that a pure magnetite phase remains in the sample at a concentration of about 15(2%). From chemical analysis, this conclusion leads us to infer a complete reduction of the iron of Fe^{2+} in the lithiated particles ($x = 2$). However, it is not possible to check this inference with an accurate Li concentration from the x-ray diffraction because the low scattering factor of Li means that a variation in the Li concentration may give similar R_{wp} factors.

This latter fact has been tested for $x = 1$ and 0.5, which give R_{wp} values of 15.56 and 15.77, respectively. Therefore, additional measurements are required in order to get new information about the actual Li content of the lithiated particles. For this, we have the isomer shifts obtained by Mössbauer data; see below.

Inspection of the difference pattern in Fig. 3 reveals a remarkable feature that should be mentioned. It is apparent that at 21.28°, 31.74°, and 34.08° (2θ) some weak lines exist that cannot be indexed on the basis of the *Fd* 3*m* space group. It may be argued that these lines correspond to impurities in the sample; however, the fact that they can be indexed very approximately as (200), (221), and (310) reflections when

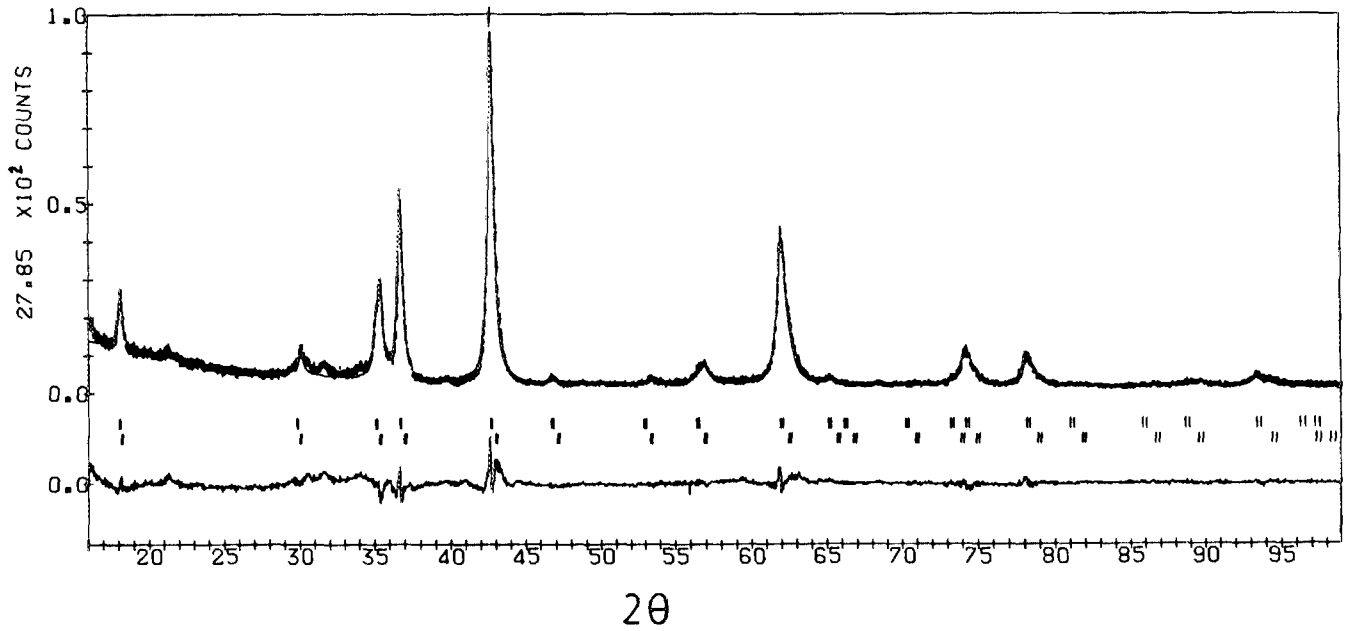

FIG. 3. X-ray diffraction pattern for $Li_xFe_3O_4$, fitted with model (iv).

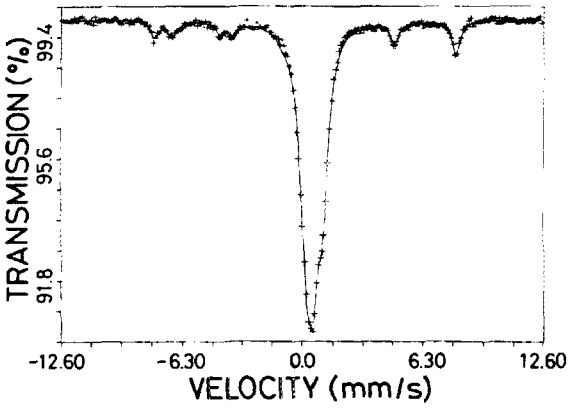

FIG. 4. Mössbauer spectrum of $Li_xFe_3O_4$ at 300 K.

using the fitted lattice parameter suggests some sort of superstructure has been established. An ordering of Li and Fe on 16*c* sites of the *Fd* 3*m* space group could reduce the symmetry to a tetragonal space group.

MÖSSBAUER SPECTROSCOPY DATA

The Mössbauer spectra of our $Li_{1.7}Fe_3O_4$ sample have been recorded at room temperature and 4.2 K in order to get some new structural and magnetic information. Figure 4 shows the room-temperature Mössbauer spectrum. The more relevant characteristic of this spectrum is the coexistence of a nonmagnetically ordered phase together with an ordered one. This spectrum has been initially fitted with a superposition of two sextets together with two broad single lines. In Table II we summarize the Mössbauer parameters obtained from the fit.

Inspection of these data shows that the Mössbauer parameters of the magnetic phase are very close to those observed for the room-temperature standard magnetite [isomer shift (IS) = 0.25 and 0.65 mm/s, hyperfine magnetic field (HF) = 493 and 460 kOe (Ref. 16)]. Therefore we can assign these two sextets to the nonlithiated magnetite phase in our sample. In addition, from the percentage of their area in the spectrum the fraction of magnetite in the sample can be calculated if equivalent recoil-free fractions are assumed for all iron nuclei. With this assumption, the concentration of magnetite is found to be about 16%, in remarkably good agreement with the x-ray-diffraction result.

On the other hand, the fit of the two inner single lines has led to very broad lines [full width at half-maximum (FWHM) = 0.90 and 0.55 mm/s]. The line broadening indicates that there may be some line splitting present that was unresolved by the large-velocity range used in the measurement. Therefore, the room-temperature spectrum was recorded again in a velocity range $\pm$ 3 mm/s in order to increase the resolution of the central part. Figure 5(a) shows the result; it does not reveal any additional structure that could improve the fitting procedure.

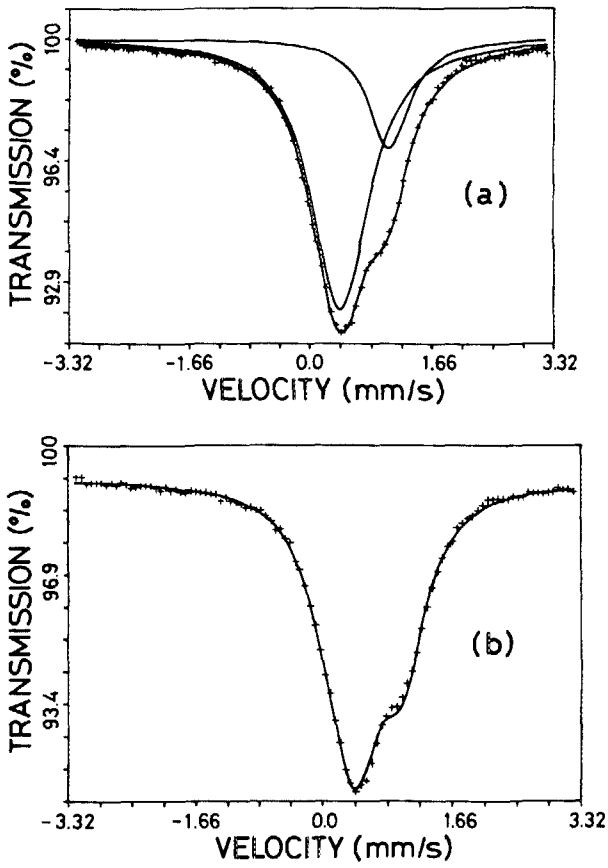

FIG. 5. Room-temperature Mössbauer spectrum fitted with (a) two single lines and (b) two quadrupole doublets with intensity ratio 1:2.

The spectrum of Fig. 5(a) was initially fitted with a superposition of two broad single lines as was done for the high-velocity spectrum. The results, Table III(a), are similar to those reported in Table II.

If two quadrupolar splittings are introduced to account for the line broadening, an appreciable reduction in χ^2 is obtained [see Table III(b)] and the IS values are significantly altered. More significant is a reversal in the relative intensities of the lines and an intensity ratio of about 2, which

TABLE II. Parameters obtained from the room-temperature Mössbauer spectrum. IS, QS, HF, FWHM, *A*, and χ^2 are the isomer shift (vs α-Fe), quadrupole splitting, hyperfine magnetic field, half-width, percentage of the total area, and the quality-of-fit factor, respectively.

IS (mm/s)	QS (mm/s)	HF (kOe)	FWHM (mm/s)	*A* (%)	χ^2
0.24(6)	0.00(5)	499(5)	0.32(9)	5.3(2.5)	
0.73(6)	0.00(5)	472(5)	0.77(9)	11.1(2.0)	
0.52(1)	---	---	0.92(2)	65.4(3.0)	2.60
1.19(2)	---	---	0.57(4)	18.2(3.0)	

TABLE III. Parameters obtained from the room-temperature Mössbauer spectrum. The symbols have the same meaning as in Table II.

	IS (mm/s)	QS (mm/s)	FWHM (mm/s)	*A* (%)	χ^2
(a)	0.51(1)	---	0.91(2)	77(3)	1.51
	1.16(1)	---	0.67(4)	33(3)	
(b)	0.39(5)	0.32(10)	0.71(7)	39(3)	1.11
	0.86(4)	0.56(7)	0.71(7)	61(3)	
(c)	0.38(4)	0.32(10)	0.73(7)	33(3)	1.45
	0.83(4)	0.58(7)	0.73(7)	66(3)	

indicates that one of the lines comes from a set of sites having twice the iron occupancy of the other set of iron-occupied sites. Since the structural model has, per molecule, two Fe atoms in sites 16*d* and one Fe atom in site 16*c*, it follows that the intensity ratio should be 2; and the line of larger intensity should be associated with sites 16*d* and that of smaller intensity with 16*c* sites. Therefore we eliminate a variable in our fit, shown in Fig. 5(b), by constraining the intensity ratio to be exactly 2; the resulting parameters are given in Table III(c). The only change between Table III(b) and III(c) is a small increase in χ^2 due to the decrease in the number of adjustable parameters.

From the discussion to this point, we should be able to interpret the spectrum of Fig. 5(b) on the basis of the structural formula

$$(\mathrm{Li}_{x-1})_{8a}(\mathrm{LiFe}^{3+}_{1-x+y}\mathrm{Fe}^{2+}_{x-y})_{16c}[\mathrm{Fe}^{2+}_{1+y}\mathrm{Fe}^{3+}_{1-y}]\mathrm{O}_4. \quad (1)$$

Moreover, from chemical analysis and the observation of about 15% Fe_3O_4 in our sample, we were led to expect a complete reduction of the iron in the lithiated phase ($x=2$ and $y=1$). We now ask whether this reduction is consistent with the measured IS values.

Gupta *et al.*[20] have compiled IS data for high-spin Fe^{3+} and Fe^{2+} iron ions in octahedral and tetrahedral sites of several oxides, mainly spinels. For high-spin Fe^{3+} ions in octahedral sites, they found room-temperature IS values with respect to α-Fe in the range $1.1<\mathrm{IS}<1.3$ mm/s; for octahedral-site Fe^{3+} ions a range $0.2<\mathrm{IS}<0.4$ mm/s. Where there is fast electron transfer between Fe^{2+} and Fe^{3+} ions (hopping time $\tau_h<10^{-8}$ s), a mean IS is observed. For a mixed-valence, high-spin configuration Fe^{m+}, on octahedral sites, an empirical formula

$$\mathrm{IS}_m=(2.85-0.85m\pm0.1)\ \mathrm{mm/s} \quad (2)$$

may generally be used if the mean value is $2\leqslant m\leqslant 3$.[21]

In magnetite, for example, an $\mathrm{IS}_{16d}=0.67(4)$ mm/s falls within the empirical range $\mathrm{IS}_{2.5}=0.72\pm0.1$ mm/s obtained from Eq. (2). From Table III(c), the measured IS values $\mathrm{IS}_{16c}=0.38(4)$ mm/s and $\mathrm{IS}_{16d}=0.83(4)$ mm/s falls significantly below the anticipated value $\mathrm{IS}_{2+}=1.15\pm0.1$ mm/s. In fact, application of Eq. (2) would give mean valences of $Fe^{2.9\pm0.1}_{16c}$ and $Fe^{2.4\pm0.1}_{16d}$. The minimum valence states $m=2.8+$ and $2.3+$, corresponding to maximum lithiation, give $y=0.4$ and $x=0.6$ in Eq. (1), which corresponds to the structural formula

$$(\mathrm{Li}_{0.6}\square_{0.4}\mathrm{Fe}^{2.8+})_{16c}[\mathrm{Fe}^{2.3+}_2]_{16d}\mathrm{O}_4. \quad (3)$$

This result is clearly incompatible with the chemical analysis.

On the other hand, lithiation of Fe_3O_4 at 400 °C was found to result in the extrusion of metallic iron.[11] Therefore we are forced to reconsider the possibility that some iron has been extruded in our room-temperature lithiation.

The following observations argue against the presence of any metallic iron in our sample:

(1) Figure 4 shows no evidence of α-Fe, which has a well-known Mössbauer spectrum. At room temperature, the most intense, more external lines are at 5.22, 2.97, -3.19, and -5.44 mm/s.

(2) Were the iron present in such fine-particle form that it was paramagnetic at room temperature, a single-line Mössbauer spectrum placed at -0.11 mm/s should appear; no line is present at this position in Fig. 5. It was not possible to obtain a meaningful fit to the data with a line introduced at this position.

(3) No extra line belonging to α-Fe appears in the x-ray-diffraction pattern. If present as an amorphous phase, the iron occupancy of the 16*c* sites of the lithiated phase should be reduced. However, fitting of the complete x-ray pattern with the Fe/Li ratio on 16*c* sites allowed to vary gave convergence for a 16*c*-site occupancy $\mathrm{Fe}_{1.075}\mathrm{Li}_{0.925}$.

Since there is no evidence of extruded iron, we have three possibilities to interpret our Mössbauer data: (a) to question the chemical analysis for lithium, which, however, is consistent with the room-temperature electrochemical evidence[10] for a lithiation limit corresponding to $Li_2Fe_3O_4$, i.e., to $x=2$ in Eq. (1), (b) to assume that Eq. (2) is not applicable to the lithiated compound, or (c) to assume that one exposure of our sample to air, Li has diffused out of the lithiated particles into a layer of physisorbed oxygen. As there is extensive evidence in the literature[21] for the validity of Eq. (2) in the presence of an ion such as Li^+, we are forced to conclude that our sample has become lithiated on exposure to air. The fact that Li is inserted at room temperature shows that the sample can also be readily oxidized by room-temperature delithiation. It would appear that smaller particles with a larger surface-to-volume ratio may be completely delithiated, the Fe^{3+} in 16*c* sites returning to the tetrahedral 8*a* positions for $x<x_c$; other particles appear to delithiate to a composition $x\simeq0.5$ in which the iron on 16*c* sites are essentially all oxidized to Fe^{3+} and may be ordered.

An important feature of the room-temperature spectra is the absence of magnetic ordering in the lithiated phase. In the spinel phase Fe_3O_4, the dominant magnetic interaction responsible for the high Curie temperature is the antiferromagnetic Fe_A-O-Fe_B (the 8*a*-O-16*d*) interaction via half-filled σ-bonding *d* orbitals.[21] In the lithiated phase, diplacement of the 8*a*-site iron to 16*c* sites eliminates this interaction, but it introduces similar 180° 16*c*-O-16*d* interactions.

In MnO and NiO, which have rocksalt structure, these antiferromagnetic 180° *M*-O-*M* interactions induce an antiferromagnetic coupling between adjacent (111) cation planes. The cation ordering in the lithiated phase has three 16*d* to one 16*c* sites on one set of (111) planes and three 16*c* to one 16*d* sites on the alternate set of (111) planes. It follows that a ferrimagnetic order should be observed below a T_C in the lithiated phase. Moreover, the number of 16*c*-O-16*d* interactions is the same as the number of 8*a*-O-16*d* interactions, so a decrease of T_C in the lithiated phase would reflect primarily a decrease in the magnitude of the Fe-O-Fe interactions.

The Fe-O-Fe superexchange interaction varies as λ_σ^4, where $\lambda_\sigma=|b^{ca}|^2/\Delta E$ is the covalent-mixing parameter associated with the σ-bonding *d* orbitals.[21] The energy-transfer (resonance) integral $b^{ca}_\sigma=(\psi_d,H'\psi_p)\simeq\epsilon(\psi_d,\psi_p)$ is proportional to the overlap of the cation-*d* and anion-*p* wave functions; the energy difference ΔE is the energy required to transfer an electron from the anion orbital ψ_p to the cation

orbital ψ_d. For an Fe^{3+} ion, the acceptor ψ_d orbital lies at the $E^0(Fe^{3+}/Fe^{2+})$ redox potential in the solid; for an Fe^{2+} ion it is at the $E^0(Fe^{2+}/Fe^{+})$ redox energy, which is considerably higher. Therefore, reduction of the Fe^{3+} ion to Fe^{2+} by lithiation can be expected to reduce significantly the strength of the Fe-O-Fe interactions, and indeed the Néel temperature of antiferromagnetic $Fe_{1-\delta}O$ is only $T_N = 198$ K. In our sample, the ordering temperature is about 150 K, only slightly lower than the corresponding to T_N of $Fe_{1-\delta}O$, where the number of nearest neighbors is higher than the number of 16*c*-O-16*d* interactions due to the partial occupancy of 8*a* sites by nonmagnetic ions. Therefore, we should conclude that the reduction of the strength of Fe(16*c*)-O-Fe(16*d*) interactions due to the complete reduction of Fe^{3+} ions has not taken place, thus supporting the Mössbauer results. However, we must anticipate a magnetic ordering within the lithiated phase below room temperature, and we can anticipate that the peculiar cationic ordering will lead to ferrimagnetism with a spontaneous magnetization.

The Mössbauer spectrum at 4.2 K is shown in Fig. 6. The six-finger pattern reveals a magnetic ordering of the lithiated phase as well as the magnetite phase at this temperature. Because of the superposition of the very complex low-temperature spectrum of magnetite onto an even more complex spectrum for the lithiated phase, it is difficult to derive an accurate and meaningful fit of the 4.2-K spectrum. The Mössbauer parameters given in Table IV were obtained from a fit done with only two sextets, but with a Lorentzian distribution of hyperfine magnetic fields.

Although the IS values are higher than those obtained at room temperature for the paramagnetic component of the spectrum, the differences (0.11 and 0.07 mm/s) are smaller than those predicted by the second-order Doppler shift [$\sim 7.1\times10^{-4}$ (mm/s)/K]. If we assume that the electronic relaxation $Fe^{2+}\rightarrow Fe^{3+}$ has been quenched due to the temperature lowering, we may interpret the 0.497- and 0.90-mm/s IS value as corresponding to Fe^{3+} and Fe^{2+} ions, respectively. On the basis of this assumption, the ratio of the areas of both sextets (53/47 = 1.14) should give the ratio of Fe^{2+}/Fe^{3+} in the sample. This result is in excellent agreement with the compositional formula $Li_{0.6}Fe^{3+}_{1.4}Fe^{2+}_{1.6}O_4$ deduced in Eq. (3) from the isomer shifts of the room-temperature spectrum. In addition, the smaller HF and larger quadrupole splitting (QS) obtained for the sextet with higher isomer shift also support the Fe^{2+} assignment.

It is clear that if the magnetite contribution to the spectrum had been included, the fit would be improved. However, due to the lack of resolution and the complexity of the low-temperature magnetite spectrum, no reliable fit could be obtained. The large line broadening and the DHF reflects the contribution of the impurity phase.

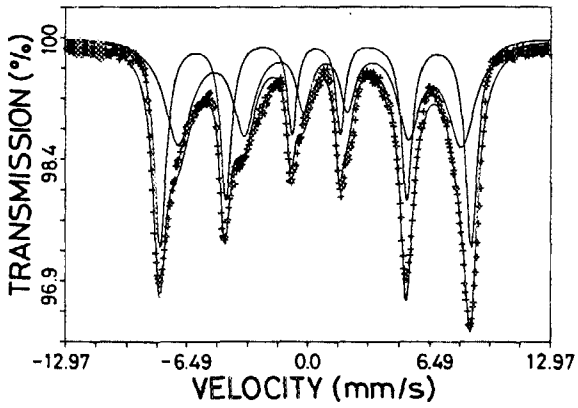

FIG. 6. Mössbauer spectrum at 4.2 K.

MAGNETIZATION RESULTS

The magnetization (M) has been measured in the temperature range $4.2 \leq T \leq 120$ K as a function of the magnetic field up to 150 kOe. Figure 7 shows the results obtained. The data have been fitted by a least-squares method to the law of approach to saturation:

$$M = \chi H + M_s[1 - (b/H^2)], \tag{4}$$

where χ is the magnetic susceptibility, M_s is the saturation magnetization, and b is a constant related to the anisotropy. In Table V, we summarize the values of χ, M_s, and b obtained from the fitting.

In our discussion of these results, we focus first on the saturation magnetic moment. According to the x-ray and Mössbauer results, we assume that our sample contains about 16% of pure magnetite with a saturation magnetic moment at 4.2 K of 4.1 μ_B.[22] The saturation magnetization of the lithiated phase at 4.2 K is then given by

$$M_s = 0.84M_s(Li_xFe_3O_4) + 0.16M_s(Fe_3O_4), \tag{5}$$

which leads to $M_s(Li_xFe_3O_4) = 21.95$ emu/g. If we assume the lithium content deduced from the Mössbauer measurements ($x = 0.6$) is correct, then the magnetic moment of the lithiated phase is $\mu = 0.93\,\mu_B$/formula unit.

If the 180° Fe-O-Fe interactions dominate to produce antiferromagnetic coupling of alternate (111) planes, then the saturation ferrimagnetic moment for a random distribution of Li and Fe on sites 16*c* would be

$$\mu_s = \mu_d - \tfrac{1}{2}\mu_c, \tag{6}$$

where μ_d is the mean magnetization to be associated with ferromagnetic coupling of the iron on 16*d* sites and μ_c is that

TABLE IV. Parameters obtained from the 4.2-K Mössbauer spectrum. DHF is the halfwidth at half-maximum of a Lorentzian distribution of hyperfine magnetic fields. The remaining symbols have the same meaning as those in Table II.

IS (mm/s)	QS (mm/s)	HF (kOe)	DHF (kOe)	FWHM (mm/s)	A (%)	χ^2
0.497(7)	−0.028(6)	514(1)	15(3)	0.54(4)	47(2)	6.53
0.90 (2)	−0.17 (1)	467(3)	62(7)	0.81(8)	53(4)	

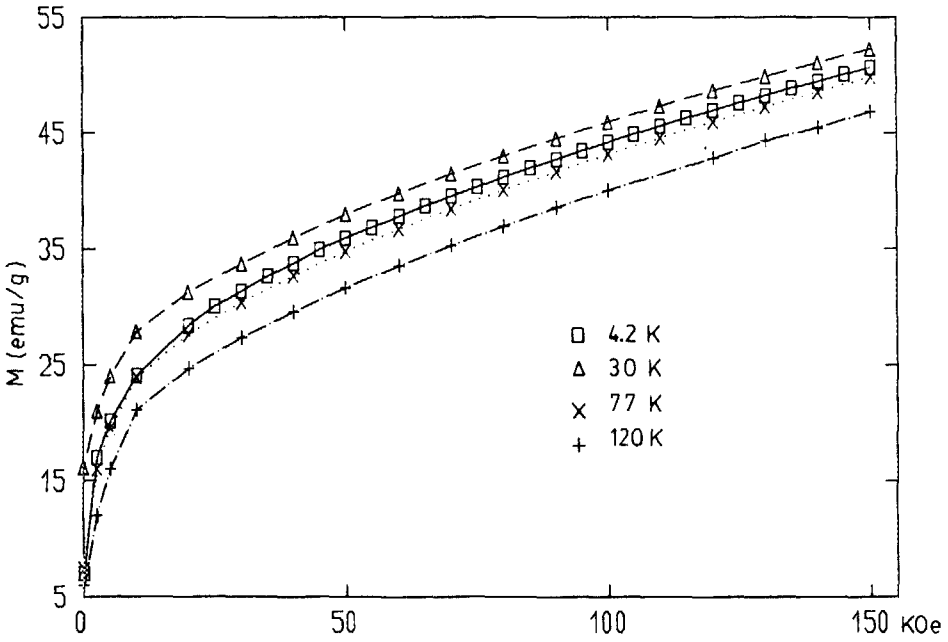

FIG. 7. Magnetization vs the external magnetic field at 4.2, 30, 77, and 120 K. The connecting lines are only eye guides.

for iron on 16*c* sites. If Eq. (6) is evaluated for Fe^{3+} on sites 16*c*, a saturation ferrimagnetic moment $\mu_s = 1.75\,\mu_B$/formula unit is predicted, which is nearly twice the observed value. The $x = 2$ value for the Li contents deduced from chemical analysis and x-ray data does not give any better μ_s value. Consequently, a canted magnetic structure should be anticipated. In fact, the large susceptibility values observed may be interpreted as a manifestation of a canting-angle dependence on the external magnetic field.

Figure 8 shows the saturation magnetic moment of the lithiated phase, obtained from the data of Table V under the assumption that the 16% magnetite will give a constant contribution—in the temperature range from 4.2 until 120 K—to the total saturation magnetic moment. This plot suggests an ordering temperature of about 150 K for the $Li_xFe_3O_4$ phase.

The fit of the $M(H,T)$ curves with the simplest form of the law of approach to saturation given by Eq. (4) allows us to obtain an estimate of the first-order anisotropy constant K_1 and the anisotropy magnetic field H_a. By the classical expressions $K_1^2 = 105bM_s/8$ and $H_a = (k_1/2)/M_s$ which hold for a cubic, uniaxial crystal,[23] we obtained $K_1 = 1.24\times10^7$ erg/cm^3 and $H_a = 35$ kOe at 4.2 K; Fig. 9 shows the fit obtained at this temperature.

At this point, it is important to realize the substantial increase of the anisotropy constant with respect to the corresponding value for pure magnetite, where K_1 is about 2.5×10^6 erg/cm^3.[24] It follows that the contribution of magnetite to the anisotropy constant of our sample should be very small and therefore that the actual value of K_1 for the lithiated phase should be very close to the measured one. The increase of the anisotropy constant and anisotropy magnetic field could be related to spin-orbit coupling at the high-spin Fe^{3+} ions in 16*d* sites, which do not have a trigonal component to the field of the type present in the spinel structure.

TABLE V. Parameters obtained from the magnetization versus magnetic field curves. χ and M_s are the susceptibility and the saturation magnetization. b is related to the anisotropy.

T (K)	$\chi(10^{-6}$ emu/g)	M_s (emu/g)	b (10^9 erg/g)
4.2	114(2)	34.1	12(1)
30.0	128(2)	33.5	4(2)
77.0	130(2)	30.5	7(2)
120.0	137(2)	25.6	2(2)

CONCLUSIONS

The Rietveld method for profile analysis of x-ray powder diffraction patterns has been used to demonstrate the presence of an unreacted phase Fe_3O_4 in a sample of $Li_xFe_3O_4$ that was exposed to air, and to obtain a quantitative measure of its concentration. However, we have not been able to elucidate the position of the Li ions in the lattice.

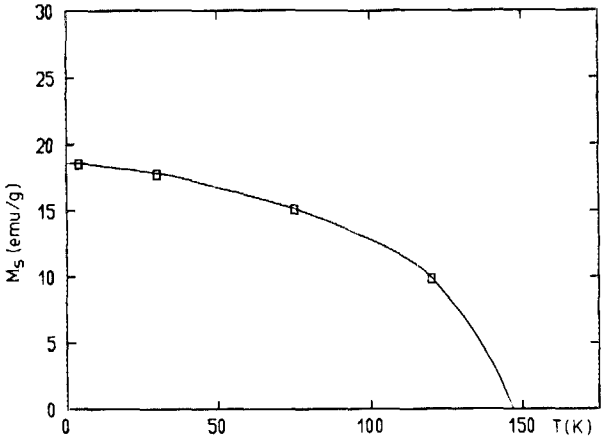

FIG. 8. Saturation magnetic moment of $Li_xFe_3O_4$ corrected for magnetite contents.

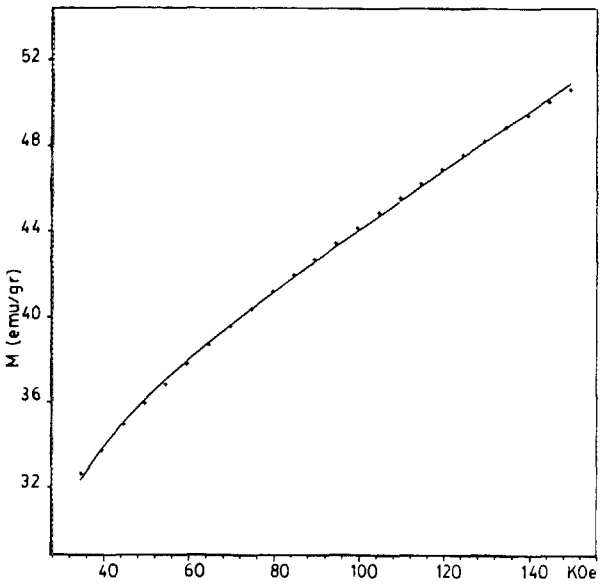

FIG. 9. Fitting of the magnetization data at 4.2 K with the law of approach to saturation.

The presence of some weak diffraction peaks closely indexable in a tetragonal lattice with the same lattice parameter as obtained from the fitting has led to the suggestion that some superstructure may exist in the lithiated phase.

The presence of pure magnetite has also been observed by Mössbauer spectroscopy. Its concentration was found to be in excellent agreement with the value obtained with the Rietveld method.

A careful inspection of the room-temperature IS values for the lithiated phase has demonstrated the incorporation of some lithium into the lattice and provided an estimation of its concentration. At room temperature there appears to be a fast electronic relaxation between Fe^{2+} and Fe^{3+} ions, but a $\tau_h > 10^{-7}$ s is found at 4.2 K. Therefore the low-temperature spectrum allows an independent estimation of the lithium incorporation, which turns out to be in good agreement with the concentration determined from the room-temperature spectrum.

The magnetization measurements have led to the conclusion that a noncollinear magnetic structure should be present in $Li_xFe_3O_4$.

Finally, we should remark that the disagreement between the Li contents determined by atomic absorption and by Mössbauer spectroscopy may be due to the presence of some undetectable lithium derivatives such as surface Li_2O.

We interpret our result to mean that iron extrusion from $Li_xFe_3O_4$ does not occur at room temperature, even for large x, but that room-temperature exposure to air oxidizes the sample via delithiation with the formation of an undetected lithium derivative, probably Li_2O, on the particle surfaces. The fact that 84% of the $Li_xFe_3O_4$ particles had $x = 0.5$ with Li_xFe^{3+} on sites 16*c* suggests that Fe^{2+} ions on sites 16*c* are the iron ions most susceptible to oxidation.

[1]A. Honders, Ph.D. thesis, University of Utrecht (1984).
[2]M. G. S. R. Thomas, P. G. Bruce, and J. B. Goodenough, Solid State Ionics **17**, 13 (1985).
[3]J. B. Goodenough, M. M. Thackeray, W. I. F. David, and P. G. Bruce, Rev. Chim. Min. **21**, 435 (1984).
[4]J. B. Goodenough, in *Proceedings of the Manganese Dioxide Electrode Symposium*, J. Electrochem. Soc. **85-4**, 77 (1985).
[5]M. R. Harrison, P. P. Edwards, and J. B. Goodenough, J. Solid State Chem. **54**, 136 (1984); **54**, 426 (1984).
[6]M. R. Harrison, P. P. Edwards, and J. B. Goodenough, Philos. Mag. **52 B**, 679 (1985).
[7]M. M. Thackeray and J. Coetzer, Mater. Res. Bull. **16**, 591 (1981).
[8]R. J. Cava, D. W. Murphy, S. Zahurak, A. Santoro, and R. S. Roth, J. Solid State Chem. **53**, 64 (1984).
[9]J. C. Hunter, J. Solid State Chem. **39**, 142 (1981).
[10]M. M. Thackeray, W. I. F. David, and J. B. Goodenough, Mater. Res. Bull. **17**, 785 (1982).
[11]M. M. Thackeray, W. I. F. David, and J. B. Goodenough, J. Solid State Chem. **55**, 280 (1984).
[12]M. M. Thackeray, W. I. F. David, and J. B. Goodenough, Mater. Res. Bull. **18**, 461 (1983).
[13]D. M. Torrie, Solid State Commun. **5**, 715 (1967).
[14]R. W. Millar, J. Am. Chem. Soc. **51**, 215 (1929).
[15]R. Bauminger, S. G. Cohen, A. Marinov, S. Ofer, and E. Segal, Phys. Rev. **122**, 1447 (1961); W. Künding and R. S. Hargrove, Solid State Commun. **7**, 223 (1969).
[16]B. J. Evans, and S. Hafner, J. Appl. Phys. **40**, 1412 (1969).
[17]D. B. Wiles and R. A. Young, J. Appl. Crystallogr. **14**, 149 (1981).
[18]R. A. Young and D. B. Wiles, J. Appl. Crystallogr. **15**, 430 (1982).
[19]N. N. Greenwood, in *Cristales Ionicos, Defectos Reticulares y Estructura* (Alhambra, Madrid, 1970).
[20]M. P. Gupta, S. M. Kanetkar, S. K. Date, A. S. Nigakevar, and A. P. B. Sinha, J. Phys. C **12**, 2401 (1979).
[21]C. Gleitzer and J. B. Goodenough, Struct. Bonding (Berlin), **61**, 1 (1985).
[22]J. Smit and H. P. I. Wijn, *Ferrites* (Wiley, New York, 1959).
[23]R. Grossinger, Phys. Status Solidi A **66**, 665 (1981).
[24]S. Chikazumi, Am. Inst. Phys. Conf. Proc. No. 29, 384 (1976).